SEMARAK ILMU PUBLISHING

Semarak Journal of Thermal-Fluid Engineering

Journal homepage:
https://semarakilmu.my/index.php/sjotfe/index
ISSN: 3030-6639

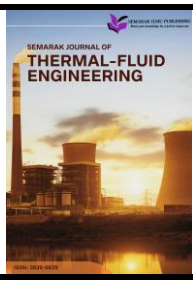

Internal Flow Through a Y-Junction Manifold

Muhammad Iqbal Zahin Arsam[1,*]

[1] Faculty of Mechanical and Manufacturing Engineering, Universiti Tunn Hussein Onn Malaysia, 86400 Parit Raja, Johor, Malaysia

ARTICLE INFO

Article history:
Received 15 October 2025
Received in revised form 12 December 2025
Accepted 16 December 2025
Available online 21 December 2025

Keywords:
Y-junction manifold; k-epsilon turbulence models; Computational Fluid Dynamics (CFD) simulation

ABSTRACT

This study examines the flow behaviour inside Y-junction manifolds, which influences the performance of ventilation, piping, and fluid distribution systems. Due to complex shapes at the branching point, flow separation, pressure loss, and uneven velocity distribution often occur, posing challenges for accurate prediction. The research evaluates three popular k-ε turbulence model variants which were Standard, RNG, and Realizable using Computational Fluid Dynamics (CFD) to assess their effectiveness in predicting internal flow characteristics. A 3D Y-junction geometry was created and meshed with an unstructured grid, followed by a grid independence study to confirm numerical accuracy. The medium mesh shows a 3.73% deviation from the finer mesh, while the coarse mesh exhibits the largest difference at 6.28%, indicating that the finer mesh provides the most stable and mesh-independent solution. Water was the working fluid, with an inlet velocity of 1 m/s and zero-gauge pressure at the outlet. The SIMPLE algorithm solved the mass and momentum equations, running simulations for each turbulence model. Results show that all three turbulence models successfully captured the general flow pattern, including symmetric velocity splitting and a consistent pressure drop across the bifurcation. However, each model exhibited different levels of sensitivity to flow structures within the junction. The Realizable k-ε model produced the clearest velocity transitions and a more defined low-velocity region along the inner curvature, indicating better resolution of separation and secondary flow. The RNG k-ε model demonstrated improved sensitivity to strain and swirling effects near the branching zone, while the Standard model generated more diffused contours with weaker separation features. Overall, the findings highlight that turbulence model selection significantly influences the accuracy of predicted internal flow characteristics. Among the three models, the Realizable k-ε formulation provided the most consistent representation under the conditions studied, making it a suitable choice for analysing pressure behaviour and flow distribution in Y-junction manifold applications.

1. Introduction

The flow behaviour within branched duct systems holds significant importance in engineering fields including HVAC, fluid distribution networks, and exhaust systems [1,2]. Y-junction manifolds

* *Corresponding author.*
E-mail address: dd220066@student.uthm.edu.my

https://doi.org/10.37934/sjotfe.7.1.1016a

are commonly used to divide incoming flow into two outlets, enabling effective distribution while maintaining compact geometry [3]. However, the flow inside such junctions is highly complex due to sudden directional changes, secondary flows generated by curvature, and variations in cross-sectional area [4]. These factors frequently cause pressure losses, uneven flow distribution, and recirculation zones, particularly at moderate to high Reynolds numbers [5]. Previous studies on branch-piping flow behaviour have demonstrated that flow imbalance in branching ducts can significantly increase system energy consumption [6] and the showed that flow separation patterns in junctions strongly influence pressure losses and flow uniformity [7].

Research on Y branch duct configurations has been conducted using both experimental and numerical approaches. The geometric parameters such as branch angle and junction curvature significantly affect pressure loss and flow uniformity [8], and separation bubbles forming near curved junction regions, which enhance turbulence levels. Numerical investigations showed that turbulence-model selection has a major impact on predicting flow separation, secondary vortices, and velocity distributions within branched ducts [9]. Many of these works highlight the widespread application of standard, RNG, and realizable k-ε turbulence models in internal duct-flow simulations [10]. The resolution of the mesh significantly affects the ability to capture recirculation zones and secondary flow structures, highlighting the necessity of mesh-independence testing in CFD studies.

Despite these advances, several gaps remain. Many previous investigations focused primarily on large-scale piping or T-junction systems rather than compact Y-junction geometries commonly used in HVAC applications. Furthermore, some studies did not include mesh-independence validation, which can compromise numerical accuracy [11]. The combined influence of inlet velocity, pressure drop, and flow separation in small Y-junction manifolds also remains insufficiently explored [12], indicating the need for a more detailed CFD investigation focused specifically on internal flow behaviour in Y-branch configurations.

This study aims to analyse the internal flow behaviour within a Y-junction manifold by evaluating pressure distribution along the junction, examining velocity profiles and symmetry of flow separation, and confirming the reliability of the simulation through a grid independence assessment. These objectives support a clearer understanding of how the Y-junction geometry affects overall fluid behaviour in duct systems.

2. Methodology

2.1 Geometry of Y-Junction Pipe

The geometry was created directly within ANSYS Design Modeler using its built-in parametric modelling tools to generate a modular Y-junction configuration. The model employed a standard circular duct design commonly used in ventilation and piping systems, with a main inlet duct of 100 mm internal diameter and 2000 mm straight length leading to the junction. Both outlet branches had the same diameter and length of 2000 mm to ensure proper downstream flow development, and the bifurcation angle was set at 45° [13], following typical industrial Y-junction designs aimed at minimizing pressure loss and flow separation [14]. Figure 1 presents a schematic diagram of the final geometric setup, clearly depicting the locations of the main inlet and the two outlet branches.

The geometry depicts the complete setup used in the simulations, featuring a straight inlet section, symmetrical branches, and a specified bifurcation angle. This arrangement allows realistic flow separation and redistribution as the flow splits into the two outlet channels.

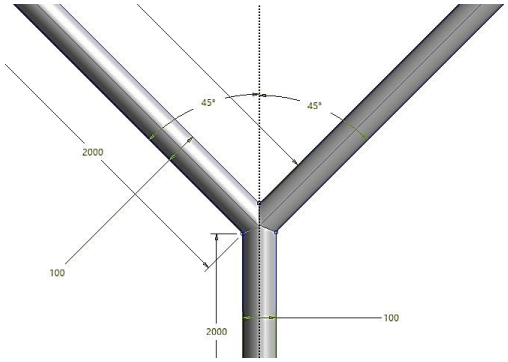

Fig. 1. Y-junction geometry showing the inlet duct, bifurcation angle of 45°, and outlet branches

2.2 Mesh Generation and Grit Independence Test

The computational mesh was created in ANSYS Meshing by using a combination of global and local controls to accurately capture the Y-junction geometry. A body sizing control was applied to the entire fluid domain to manage the overall element size, ensuring a uniform mesh distribution across the inlet duct, bifurcation area, and outlet branches. The patch conforming algorithm was used to generate the mesh, allowing it to closely follow the original geometric boundaries and align properly around curved surfaces [15]. Tetrahedral elements were generated for the mesh due to their effectiveness in discretizing complex 3D domains where multiple surfaces intersect, such as in the junction region. To ensure mesh-independent results, a systematic study on grit independence test was carried out as shown in Table 1. Three mesh densities (coarse, medium, and fine) were evaluated by varying the global element size.

Figure 2 illustrates the final mesh configuration generated using the Patch Conforming algorithm. The tetrahedral elements ensure uniform discretization across the inlet, junction, and outlet areas, allowing the solver to accurately resolve the complex flow patterns at the bifurcation. The mesh maintains a consistent density thanks to the body sizing control, which manages element distribution along the full length of the duct.

Table 1
Grid independence test summary

Mesh level	Element size (mm)	Pressure inlet (Pa)	Total number of nodes
Coarse	10.0	44.499	80371
Medium	9.0	46.228	108642
Finer	8.0	49.236	151464

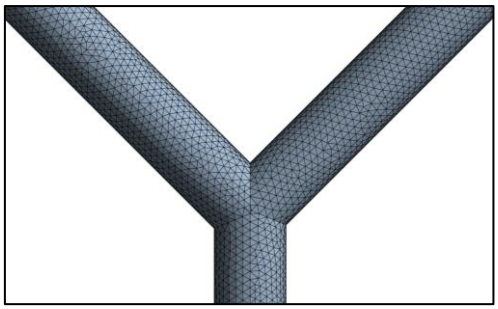

Fig. 2. Mesh distribution generated using body sizing, patch conforming algorithm, and tetrahedral elements

2.3 Boundary Conditions and Material Setup

The simulation was set up as a steady-state, incompressible internal flow problem. Four named selections (Inlet, Outlet 1, Outlet 2, and Wall) were designated within the domain to consistently apply boundary conditions. A uniform velocity of 1 m/s was applied at the Inlet, representing a typical low-speed internal pipe flow [16]. Outlet 1 and Outlet 2 were defined as pressure outlets with zero-gauge pressure, allowing fully developed flow to exit without restrictions.

All duct surfaces were treated as no-slip walls, meaning the fluid velocity relative to the solid boundary was zero. This is a common assumption for Newtonian fluids and is essential for accurately capturing velocity gradients near the walls. The working fluid was liquid water, assumed incompressible with constant density and viscosity, which is suitable for low-Mach-number pipe flows where density changes are minimal.

2.4 Solver Configuration and Governing Equations

The simulations were carried out using the pressure-based finite-volume solver in ANSYS Fluent. The governing equations include the continuity equation and the incompressible Navier–Stokes equations. Pressure–velocity coupling was achieved using the SIMPLE algorithm, a common iterative method for steady internal flow problems. To model turbulence, three versions of the k-ε turbulence model were used: (i) Standard k-ε model, (ii) RNG k-ε model and (iii) Realizable k-ε model. The k-ε models are popular in duct flow simulations due to their reliability and relatively low computational cost [17].

The fluid motion is governed by the Navier–Stokes equations, which include the continuity, momentum, and energy equations. These equations represent the conservation of mass, momentum (force balance), and energy within the fluid domain, describing how the fluid flows and transfers energy throughout the system.

2.4.1 Continuity equation (mass conservation)

Eq. (1) The continuity equation expresses mass conservation for incompressible flow. It ensures that the total mass entering and leaving any control volume is balanced. Because the fluid density is constant in incompressible flows, the equation simplifies to requiring that the velocity field has zero divergence [18].

$$\nabla \cdot V = 0 \tag{1}$$

2.4.2 Momentum equation (Navier–Stokes equation)

Eq. (2) show momentum equation represents Newton's Second Law applied to fluid motion. The inertial term $(\rho(V \cdot \nabla)V)$ describes the fluid's acceleration. The pressure gradient term $(-\nabla p)$ drives the fluid from regions of high to low pressure, while the viscous term $(\mu\nabla 2V)$ accounts for internal friction within the fluid. Additional forces F include the effects of turbulence modeled by the k–ε turbulence model. This equation captures the balance of forces acting on a fluid element, with inertia, pressure, viscous resistance, and turbulence contributions all playing key roles in the fluid's behavior [19,20].

$$\rho(V \cdot \nabla)V = -\nabla p + \mu\nabla 2V + F \tag{2}$$

3. Result

3.1 Grid Independence Test

The grid independence assessment was carried out using three mesh densities which are coarse, medium, and finer, as summarised in Table 2. The pressure at the inlet showed only minor variations when the mesh was refined, with the medium mesh differing by 3.73% from the finer mesh. Although the finer grid produced a slightly higher-pressure value, the improvement was not significant enough to justify the substantial increase in node count and computational cost. Therefore, the medium mesh was selected for subsequent simulations as it provides an optimal balance between accuracy and computational efficiency. The results are presented in Table 2. Static pressure at the inlet was tracked, and a difference of less than 5% between the medium and fine meshes demonstrated mesh convergence, in accordance with the criteria. Medium mesh level was selected as element size used in this case.

Table 2
Grid independence test summary

Mesh level	Element size (mm)	Total number of nodes	Pressure inlet (Pa)	Pressure outlet (Pa)	Pressure different (Pa)	Variation from fine mesh (%)
Coarse	10.0	80371	44.499	0	44.499	-
Medium	9.0	108642	46.228	0	46.228	3.73
Finer	8.0	151464	49.236	0	49.236	6.28

3.2 Velocity Contour of Three Different Model

The velocity contour obtained using the Standard k-ε model. Figure 3(a) shows that the highest velocity region forms along the centre of the inlet before splitting into the two outlet branches. A mild velocity imbalance appears near the junction, indicating limited prediction of secondary flow effects. For the RNG k-ε model, the velocity contour in Figure 3(b) displays a similar flow pattern but with clearer velocity reduction near the bifurcation walls. This indicates that the RNG model captures swirling and strained flow regions more effectively than the Standard model. The Realizable k-ε model provides the most refined velocity field, as seen in Figure 3(c). The high-velocity core remains well-defined, while the transition to the low-velocity boundary layers appears smoother. This suggests that the Realizable model better resolves shear layers and flow separation near the junction.

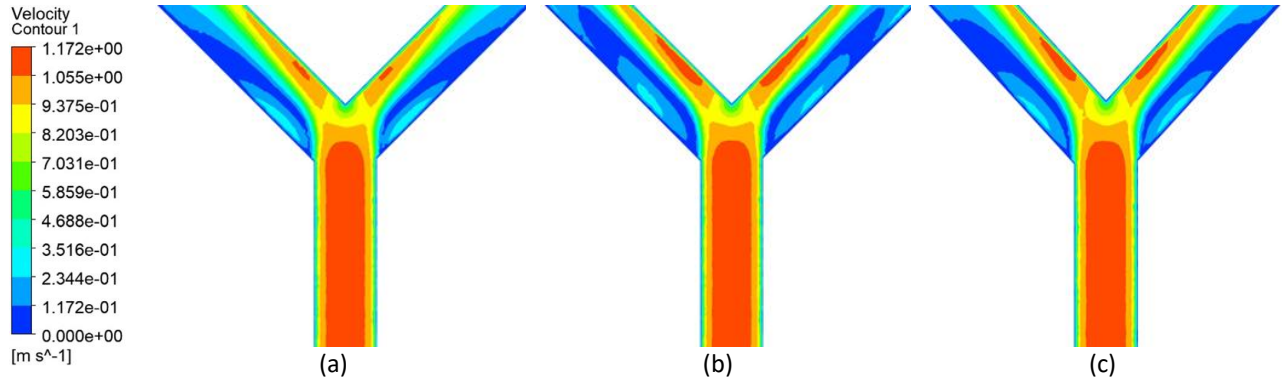

Fig. 3. Velocity contour of (a) Standard (b) RNG (c) Realizable

3.3 Pressure Contour of Three Different Model

The pressure contour using the Standard k-ε model as shown in Figure 4(a) shows a distinct pressure drop immediately after the inlet and around the bifurcation region. The pressure field appears smoothed, indicating weaker prediction of recirculation effects. In the RNG k-ε model, the pressure contour illustrated in Figure 4(b) reveals a more pronounced pressure reduction at the branching zone. The steeper gradients reflect stronger curvature-related losses, consistent with the RNG model's improved performance for rapidly strained flows. The Realizable k-ε model predicts a broader low-pressure region at the junction, as displayed in Figure 4(c). The pressure decreases more uniformly across both outlets, suggesting enhanced representation of recirculation and secondary flow structures.

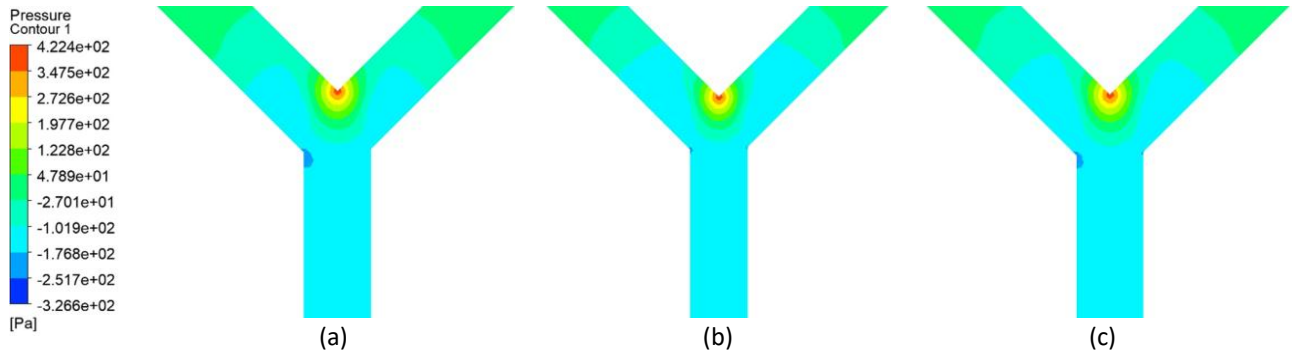

Fig. 4. Pressure contour of (a) Standard (b) RNG (c) Realizable

Overall, all three turbulence models produce similar qualitative trends, where the velocity divides symmetrically between the two outlets and the pressure consistently decreases along the Y-junction. However, notable differences arise in the predicted flow details. The Realizable k-ε model provides the most realistic representation of flow separation and delivers smoother velocity transitions near the bifurcation. The RNG k-ε model shows enhanced sensitivity to swirling and highly strained regions, resulting in sharper gradients around the junction. In contrast, the Standard k-ε model generates more diffused velocity and pressure fields due to its simpler formulation. These variations highlight the significance of selecting an appropriate turbulence model to ensure accurate prediction of internal flow characteristics in Y-junction manifolds.

4. Conclusions

The CFD results show that the Y-junction produces a clear pressure drop at the bifurcation and a symmetric velocity split between the two outlets. The grid independence test confirms that the medium mesh provides stable and reliable pressure predictions with less than 5% variation from the finer mesh. Comparison of the three k-ε models indicates that while all capture the overall flow behaviour, the Realizable model provides the smoothest and most detailed representation of velocity and pressure fields. The RNG model shows stronger sensitivity to swirling regions, whereas the Standard model produces more diffused contours. Overall, the Realizable k-ε model is the most suitable for accurately predicting flow characteristics in the Y-junction manifold.

References

[1] Ndiaye, Pape Tamsir, Goumbo Ndiaye, Oumar Drame, Omar Ngor Thiam, and Momath Ndiaye. "Computational Fluid Dynamics (CFD) of a three-inlet Y-junction duct connected to a U-bend: Influence of inlet velocities on air and

water flows subjected to cold fronts and turbulence." *World Journal of Advanced Research and Reviews* 27, no. 2 (2025): 680-92. https://doi.org/10.30574/wjarr.2025.27.2.2838

[2] Ethier, C. Ross, Sujata Prakash, David A. Steinman, Richard L. Leask, Gregory G. Couch, and M. Ojha. "Steady flow separation patterns in a 45 degree junction." *Journal of Fluid Mechanics* 411 (2000): 1-38. https://doi.org/10.1017/S0022112099008022

[3] Yoo, Geun-jong, Hoon-ki Choi, and Chul-hwan Kim. "Characteristics of turbulent flow distribution in branch piping system." *Journal of Central South University* 19, no. 11 (2012): 3208-3214. https://doi.org/10.1007/s11771-012-1397-3

[4] Nayak, Bibhuti Bhusan, and Dipankar Chatterjee. "Convective heat transfer in slurry flow in a horizontal Y-shaped branch pipe." *Powder technology* 318 (2017): 46-61. https://doi.org/10.1016/j.powtec.2017.05.036

[5] Torregrosa, Antonio J., Alberto Broatch, Luis M. García-Cuevas, and Manuel Hernández. "A study of the transient response of duct junctions: measurements and gas-dynamic modeling with a staggered mesh finite volume approach." *Applied Sciences* 7, no. 5 (2017): 480. https://doi.org/10.3390/app7050480

[6] Karuppa Raj, R. Thundil, and M. P. Dhyan Shankar. "Effect of convergent angle on flow characteristics of y-shaped diffusers using CFD." *Applied Mechanics and Materials* 592 (2014): 1909-1913. https://doi.org/10.4028/www.scientific.net/AMM.592-594.1909

[7] Sun, Bin, Quan Liu, Hongyuan Fang, Chao Zhang, Yuanbo Lu, and Shun Zhu. "Numerical and experimental study of turbulent mixing characteristics in a T-junction system." *Applied Sciences* 10, no. 11 (2020): 3899. https://doi.org/10.3390/app10113899

[8] Lin, Xinyi, Beile Zhang, Ming Zhang, Yongli Zhao, Tianwei Lai, Liang Chen, and Rong Xue. "Influence of internal flow on the performance of high-speed centrifugal pumps with a fully sealed structure." *Applied Sciences* 12, no. 10 (2022): 5263. https://doi.org/10.3390/app12105263

[9] Banerjee, Arka, and Joydeep Mazumdar. "A numerical investigation on rheological turbulent flow through a 90° mixing elbow." *Journal of Engineering and Applied Science* 71, no. 1 (2024): 209. https://doi.org/10.1186/s44147-024-00547-y

[10] Tawackolian, Karsten, and Martin Kriegel. "Validation of computational fluid dynamics simulations for determining pressure loss coefficients of ventilation components." *Building Services Engineering Research & Technology* 44, no. 3 (2023): 269-283. https://doi.org/10.1177/01436244231159537

[11] Hirani, Aslam A., and C. Udaya Kiran. "CFD simulation and analysis of fluid flow parameters within a Y-shaped branched pipe." *IOSR Journal of Mechanical and Civil Engineering, 10 (1)* (2013): 31-34. https://doi.org/10.9790/1684-1013134

[12] Haryadi, Haryadi, Sugianto Sugianto, Ali Mahmudi, and Radi Suradi Kartanegara. "A numerical study on T-reduce junction flow distribution." *Science, Technology, and Communication Journal* 2, no. 2 (2022): 55-62. https://doi.org/10.59190/stc.v2i2.208

[13] Ferziger, Joel H., Milovan Perić, and Robert L. Street. *Computational methods for fluid dynamics*. Springer, 2019. https://doi.org/10.1007/978-3-319-99693-6

[14] Li, Xin, and Shaoping Wang. "Flow field and pressure loss analysis of junction and its structure optimization of aircraft hydraulic pipe system." *Chinese Journal of Aeronautics* 26, no. 4 (2013): 1080-1092. https://doi.org/10.3901/CJME.2013.04.779

[15] Suteria, Naureen S., Mehdi Nekouei, and Siva A. Vanapalli. "Microfluidic bypass manometry: highly parallelized measurement of flow resistance of complex channel geometries and trapped droplets." *Lab on a Chip* 18, no. 2 (2018): 343-355. https://doi.org/10.1039/C7LC00889A

[16] Richardson, S. "On the no-slip boundary condition." *Journal of Fluid Mechanics* 59, no. 4 (1973): 707-719. https://doi.org/10.1017/S0022112073001801

[17] Shaheed, Rawaa, Abdolmajid Mohammadian, and Hossein Kheirkhah Gildeh. "A comparison of standard k–ε and realizable k–ε turbulence models in curved and confluent channels." *Environmental Fluid Mechanics* 19, no. 2 (2019): 543-568. https://doi.org/10.1007/s10652-018-9637-1

[18] Kundu, Pijush K., Ira M. Cohen, and David R. Dowling. 2015. *Fluid Mechanics*. 6th ed. Cambridge, MA: Academic Press.

[19] Ahammad, Jalal M., Mohammad Azizur Rahman, Stephen D. Butt, and Jahrul M. Alam. "Integrated wellbore-reservoir modeling based on 3D Navier–Stokes equations with a coupled CFD solver." *Journal of Petroleum Exploration and Production Technology* 14, no. 8 (2024): 2539-2554. https://doi.org/10.1007/s13202-024-01833-4

[20] Tougma, Jean Luc Wendkouni. "Method of Analytical Resolution of the Navier-Stokes Equations." *Open Journal of Fluid Dynamics* 13, no. 5 (2023): 226-231. https://doi.org/10.4236/ojfd.2023.135017